Atkinson Index Detector for Spectrum Sensing

Dayan Adionel Guimarães

Abstract—A new approach for designing detectors for cooperative spectrum sensing has recently been developed. It applies an incoming inequality index, which is normally used in economic and social sciences, to build a test statistic that operates on the entries of the received signal sample covariance matrix. The first detector designed using this approach was the Gini index detector (GID). This letter devises the Atkinson index detector (AID), which is shown to outperform the GID in many situations, with the special attribute of attaining a time complexity that grows linearly with the number of secondary users.

Index Terms—Atkinson index, cognitive radio, dynamic spectrum access, Gini index, spectrum sensing.

I. INTRODUCTION

THE proliferation of wireless communication systems in recent years has resulted in scarcity of available radio frequency (RF) spectrum. This scarcity can be credited to the implementation of fixed spectrum allocation policies, where a network of primary users (PUs) holds exclusive rights to utilize specific RF bands. However, research indicates that numerous allocated RF bands remain underutilized in particular regions and time periods, leading to inefficient spectrum utilization [1].

The landscape of RF spectrum scarcity is anticipated to deteriorate with the expansion of Internet of Things (IoT) and 5G networks, and the emergence of 6G networks. These advancements will demand larger bandwidths and intensify competition for the already constrained spectrum resources [1].

A potential remedy for the issue of inefficient spectrum utilization involves the implementation of cognitive radio (CR) networks. These networks enable the identification of vacant bands resulting from the variable occupancy of the primary network spectrum in both time and space [2]. In such scenarios, a dynamic spectrum access (DSA) policy can be implemented, allowing cognitive terminals of secondary users (SUs) to opportunistically utilize unoccupied frequency bands. This approach, known as spectrum sensing [1], [3]–[5], employs techniques with or without the aid of a database of RF spectrum occupancy to detect spectral gaps, commonly referred to as whitespaces or spectrum holes.

While individual spectrum sensing performed by each SU may be susceptible to impairments such as multi-path fading, signal shadowing and hidden terminals, cooperative spectrum sensing (CSS) addresses these issues by employing multiple SUs. CSS aims to enhance the accuracy of decisions concerning the occupancy state of the sensed band by leveraging collaborative efforts among SUs.

This article considers a centralized approach to CSS with data fusion, wherein samples of the received signal from SUs are transmitted to a fusion center (FC). At the FC, these samples are used to calculate a test statistic, which is then compared with a decision threshold to yield a global decision regarding the occupancy state of the monitored band.

There is a vast list of detection techniques for spectrum sensing, from the well-known energy detection to modern solutions based on neural networks, machine learning and artificial intelligence, going through cyclo-stationary feature and eigenvalue-based detection strategies [5].

Recently, an incoming inequality index was proposed as a novel and promising detector design approach [6]. This type of index is commonly used in economic and social sciences to measure income or wealth inequality among groups or populations. Using this approach for the first time, the Gini index detector (GID) has been derived in [6], where the Gini index formula has been adapted to operate on the elements of the received signal sample covariance matrix (SCM). The resultant GID attained low complexity, robustness against variations in signal and noise power levels, and exhibited the constant false alarm rate (CFAR) property, yet outperforming several state-of-the-art detectors in many practical situations.

This letter devises the new Atkinson index detector (AID). As the name suggests, the detector is based on the Atkinson index [7] for income inequality measurement. It is shown that the AID is robust against variations in signal and noise powers, attains the CFAR property, and has low time complexity. Moreover, the AID performs close to the GID, but exhibits a latency far below its predecessor. The performances of both detectors are addressed by means of computer simulations modeled according to a practical-appealing system model encompassing distance-dependent received signal powers, nonuniform noise levels across the SUs, multi-path fading with variable line-of-sight condition, and a consistent procedure to calibrate the signal-to-noise ratio (SNR). Additionally, the model is subjected to variations of the main system parameters that govern the spectrum sensing performance, allowing for a realistic assessment of AID and GID.

The subsequent sections of this letter are structured as follows: Section II outlines the models for signals, noise and channels. The AID test statistic is devised in Section III. Section IV focuses on numerical results and discussions, while Section V provides the concluding remarks for the work.

D. A. Guimarães is with the National Institute of Telecommunications (Inatel), Santa Rita do Sapucaí, MG, Brazil, e-mail: dayan@inatel.br. ORCID 0000-0002-1304-792X.

II. SIGNAL, NOISE AND CHANNEL MODELS

The model employed for centralized CSS with data fusion is primarily based on [8]. Thus, some details are omitted for conciseness. Spectrum sensing is conducted by m SUs, each gathering n samples of the PU signal over a sensing interval. The collected samples are transmitted to the FC through an error-free control channel, thereby forming the sample matrix $\mathbf{Y} \in \mathbb{C}^{m \times n}$, which is given by

$$\mathbf{Y} = \mathbf{h}\mathbf{x}^{\mathrm{T}} + \mathbf{V}, \qquad (1)$$

where the vector $\mathbf{x} \in \mathbb{C}^{n \times 1}$ contains the samples of the PU signal, modeled as complex Gaussian random variables with zero mean. The channel vector $\mathbf{h} \in \mathbb{C}^{m \times 1}$ comprises elements h_i that denote the channel gains between the PU transmitter and the ith SU, for $i = 1, \dots, m$. The temporal variation of these gains reflects the fading effect resulting from multi-path propagation and mobility of the SUs. Specifically, $\mathbf{h} = \mathbf{G}\mathbf{a}$, where $\mathbf{G}$ is a gain matrix to be defined subsequently, and $\mathbf{a} \in \mathbb{C}^{m \times 1}$ is a vector composed of complex Gaussian random variables $a_i \sim \mathbb{CN}[\sqrt{K/(2K+2)}, 1/(K+1)]$, where $K = 10^{K^{(\mathrm{dB})}/10}$ is the Rice factor of the channels between the PU and SUs, with $K^{(\mathrm{dB})} = 10\log_{10}(K)$ denoting its dB value.

Based on the findings reported in [9], it was realized that $K^{(\mathrm{dB})}$ is a random variable, well characterized by a Gaussian distribution with mean of μ_K and standard deviation of σ_K, both expressed in decibels. The typical values of μ_K and σ_K are determined based on the signal propagation characteristics influenced by the environment. For instance, in urban areas $\mu_K = 1.88$ dB, $\sigma_K = 4.13$ dB. In rural or open areas, $\mu_K = 2.63$ dB, $\sigma_K = 3.82$ dB are common, while suburban regions have $\mu_K = 2.41$ dB, $\sigma_K = 3.84$ dB [9].

The received signal power levels at the SUs can vary in magnitude and over time due to differences in the distances between the PU transmitter and the SUs, as well as variations in these distances across different sensing events resulting from the movement of the SUs. In such scenario, the previously mentioned gain matrix $\mathbf{G} \in \mathbb{R}^{m \times m}$ is expressed as $\mathbf{G} = \mathrm{diag}(\sqrt{\mathbf{p}/P_{\mathrm{tx}}})$, where $\mathbf{p} = [P_{\mathrm{rx}1}, \dots P_{\mathrm{rx}m}]^{\mathrm{T}}$ represents the vector of PU signal powers received by the m SUs, with $[\cdot]^{\mathrm{T}}$ indicating transposition. Here, P_{tx} denotes the PU's transmission power in watts, and $\mathrm{diag}(\cdot)$ is a diagonal matrix with its diagonal elements coming from the vector argument.

The log-distance path loss prediction model [10] is employed in this context to compute the received signal power at the ith SU, in watts, yielding

$$P_{\mathrm{rx}i} = P_{\mathrm{tx}} \left(d_0/d_i\right)^{\eta}, \qquad (2)$$

where d_0 represents a reference distance situated in the far-field region of the transmitting antenna, d_i denotes the distance between the PU and the ith SU, and η is the path loss exponent. All distance measurements are specified in meters.

Discrepancies and fluctuations in noise powers at the SUs' receivers may arise owing to temperature fluctuations, disparities among front-ends, and undesired signals entering the receivers and contributing to the noise floor. To characterize such conditions, the elements of the ith row of the matrix $\mathbf{V} \in \mathbb{C}^{m \times n}$ outlined in (1) are modeled as zero-mean Gaussian random variables with variance

$$\sigma_i^2 = (1 + \rho u_i)\bar{\sigma}^2, \qquad (3)$$

where u_i represents a realization of a uniform random variable U_i within the interval $[-1, 1]$, $\bar{\sigma}^2$ is the average noise power at the SUs, and $0 \leq \rho < 1$ denotes the fraction of variation in the noise power σ_i^2 around $\bar{\sigma}^2$.

The instantaneous SNR across the SUs, γ, is a random variable due to its dependence on σ_i^2 and d_i, both of which are random. Based on (2) and (3), a realization of γ is

$$\gamma = \frac{1}{m} \sum\nolimits_{i=1}^{m} \frac{P_{\mathrm{tx}} (d_0/d_i)^{\eta}}{(1 + \rho u_i)\bar{\sigma}^2}. \qquad (4)$$

Hence, the average SNR of the SUs is determined by $\mathrm{SNR} = \mathbb{E}[\gamma]$, where $\mathbb{E}[\gamma]$ denotes the expected value of γ. To establish this SNR model, we initially compute the expected value of γ', defined for $\bar{\sigma}^2 = 1$ and $\{d_i\}$. It can be demonstrated [8] that this expected value is given by

$$\mathbb{E}[\gamma'] = \ln\left(\frac{1+\rho}{1-\rho}\right) \frac{1}{2\rho m} \sum\nolimits_{i=1}^{m} P_{\mathrm{rx}i} \qquad (5)$$

for $0 < \rho < 1$, and for $\rho = 0$ it is given by

$$\mathbb{E}[\gamma'] = \frac{1}{m} \sum\nolimits_{i=1}^{m} P_{\mathrm{rx}i}. \qquad (6)$$

As $\mathrm{SNR} = \mathbb{E}[\gamma] = \mathbb{E}[\gamma']/\bar{\sigma}^2$, the calibrated noise level is

$$\bar{\sigma}^2 = \mathbb{E}[\gamma']/\mathrm{SNR}. \qquad (7)$$

This value of $\bar{\sigma}^2$ is plugged into (3), along with a realization u_i of the random variable U_i, to yield σ_i^2, which represents the variance of the noise samples in the ith row of $\mathbf{V}$. Fresh values of $\{\sigma_i^2\}$ are computed for each sensing event, thereby introducing temporal variability to the noise levels.

The matrix $\mathbf{Y}$ in (1) is built at the FC from the mn samples forwarded by the SUs. Under hypothesis $\mathcal{H}_1$, which means the presence of the PU signal in the sensed band, this matrix is given by $\mathbf{Y} = \mathbf{h}\mathbf{x}^{\mathrm{T}} + \mathbf{V}$. Conversely, under hypothesis $\mathcal{H}_0$, which indicates the absence of the PU signal, it follows that $\mathbf{Y} = \mathbf{V}$. From $\mathbf{Y}$, the FC computes the SCM

$$\mathbf{R} = \tfrac{1}{n}\mathbf{Y}\mathbf{Y}^{\dagger}, \qquad (8)$$

where $\dagger$ denotes conjugate transposition. Both AID and GID test statistics are built from the elements of $\mathbf{R}$.

III. ATKINSON INDEX DETECTOR

In the context of income inequality measure, let r_i represent the income of the ith population, for $i = 1, \dots, N$, and let the mean income be $\bar{r} = \sum_{i=1}^{N} r_i$. The Atkinson index [7] with the inequality aversion parameter $0 \leq \epsilon \neq 1$ is defined as

$$A_\epsilon = 1 - \frac{1}{\bar{r}}\left(\frac{1}{N}\sum\nolimits_{i=1}^{N} r_i^{1-\epsilon}\right)^{\frac{1}{1-\epsilon}}, \quad 0 \leq \epsilon \neq 1. \qquad (9)$$

Herein, this expression is adapted to the spectrum sensing scenario by replacing the incomes r_i by the elements r_{ij} of $\mathbf{R}$, yielding the AID test statistic $T_{\mathrm{AID}} = 1 - A_\epsilon$, given by

$$T_{\mathrm{AID}} = \frac{1}{\bar{r}}\left(\sum\nolimits_{i=1}^{m}\sum\nolimits_{j=1}^{m} r_{ij}^{1-\epsilon}\right)^{\frac{1}{1-\epsilon}}, \qquad (10)$$

where $\bar{r} = \sum_{i=1}^{m}\sum_{j=1}^{m} r_{ij}$. A particular case of special interest arises when $\epsilon = 0.5$, for which well-known algorithms for square root calculation can be employed to reduce the latency for computing the test statistic T_{AID}. In this case,

$$T_{\mathrm{AID}} = \frac{1}{\bar{r}}\left(\sum_{i=1}^{m}\sum_{j=1}^{m}\sqrt{r_{ij}}\right)^2$$
$$= \frac{1}{\bar{r}}\left(\sum_{i=1}^{m}\sum_{j=1}^{m}\sqrt{\frac{|r_{ij}| + \Re(r_{ij})}{2}}\right)^2, \quad (11)$$

where, to further simplify the computation, it has been exploited the fact that each complex value above the main diagonal of $\mathbf{R}$ corresponds to its conjugate below the main diagonal. This implies that the square roots of these pairs will have the same real parts but opposite imaginary parts. Consequently, the imaginary parts cancel out in the summation, resulting only in the sum of the real parts. The Appendix explains the equality used in this simplification. Additionally, as dividing by 2 in (11) does not affect the detector's performance, this division can be suppressed. Moreover, considering that the square roots operating above and below the main diagonal of $\mathbf{R}$ in the second line of (11) yield the same set of results, there can be a reduction in the total number of terms in the summations from m^2 to $m(m+1)/2$. Therefore, when $\epsilon = 0.5$,

$$T_{\mathrm{AID}} = \frac{1}{\bar{r}}\left(\sum_{i=1}^{m}\sum_{j=i}^{m}(2 - I)\sqrt{|r_{ij}| + \Re(r_{ij})}\right)^2, \quad (12)$$

where $I = 1$ for $i = j$ (elements on the main diagonal of $\mathbf{R}$), and $I = 0$ for $i \neq j$ (off the main diagonal of $\mathbf{R}$). Notice that, owed to this last simplification, only the entries on and above the main diagonal of $\mathbf{R}$ need to be computed.

IV. NUMERICAL RESULTS

The results presented hereafter have been obtained using the MATLAB code [11], from 20000 Monte Carlo simulation runs. Unless otherwise stated, $m = 6$, SNR $= -10$ dB, $\eta = 2.5$, $r = 1$ km, $d_0 = 1$ m, $P_{\mathrm{tx}} = 5$ W, PU at $(1,1)$ km, $n = 200$, $\rho = 0.5$, $\mu_K = 1.88$ dB, $\sigma_K = 4.13$ dB, $P_{\mathrm{fa}} = 0.1$.

A. CFAR property of the AID

The CFAR property of a detector refers to its ability to keep a fixed probability of false alarm, P_{fa}, irrespective of the noise power. In this case, the decision threshold is set in the detector's design phase for a target P_{fa}, and is kept unchanged no matter the noise level. Fig. 1 shows empirical probability density functions (PDFs) estimated for 20000 values of T_{AID} under hypothesis $\mathcal{H}_0$, for four randomly chosen values of $\bar{\sigma}^2$. It can be seen that the PDFs are almost identical to each other, thus maintaining P_{fa} for any predefined threshold.

B. The Gini index detector

Since the GID is the benchmark for the results presented hereafter, this subsection briefly presents its test statistic. Let r_i denote the ith element of the vector $\mathbf{r}$ formed by stacking all columns of $\mathbf{R}$, for $i = 1, \ldots, m^2$. The GID test statistic proposed in [6] is computed at the FC according to
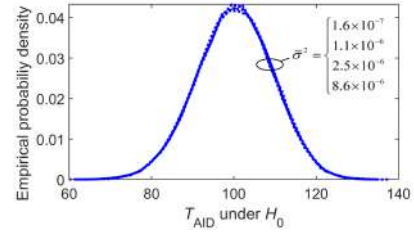

Fig. 1. Empirical PDFs of T_{AID} under $\mathcal{H}_0$.

$$T_{\mathrm{GID}} = \frac{2(m^2 - m)\sum_{i=1}^{m^2}|r_i|}{\sum_{i=1}^{m^2}\sum_{j=1}^{m^2}|r_i - r_j|}, \quad (13)$$

where the constant $2(m^2 - m)$ has been used in [6] for convenience, but it does not influence the performance of the GID detector, and can be removed.

C. Performance comparisons

As preliminary results, Fig. 2 shows the influence of the inequality aversion parameter, ϵ, of the AID on the probability of detection, P_{d}, for $P_{\mathrm{fa}} = 0.1$, and on the average run-time spent for computing T_{AID} and T_{GID}, for $m = 6$ and $m = 12$ SUs. From Fig. 2a it can be seen that $\epsilon = 0.5$ is a conservative choice, which is reinforced by the decreased run-time of the AID observed in Fig. 2b. Hence, the remaining results of this section adopts $\epsilon = 0.5$.
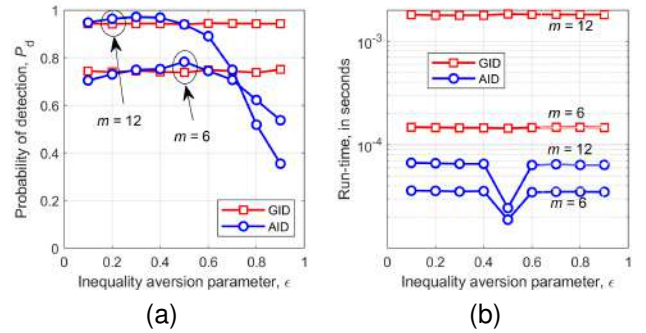

Fig. 2. (a) Probability of detection versus ϵ, and (b) run-time versus ϵ.

A closer look at the influence of m on P_{d} and run-time can be made with the help of Fig. 3. As expected, the performance improves with an increasing number of SUs, though with diminishing returns. The AID is slightly superior to the GID for smaller m, whereas the opposite happens for larger m.

Fig. 3b unveils the most attractive result, which is the much lower run-time of the AID as m gets larger. A curve fitting of the type $ax^b + c$ has been applied to the run-time measurements given in Fig. 3b, yielding $a \approx 4.9 \times 10^{-7}$, $b \approx 3.9$, and $c \approx -1.5 \times 10^{-5}$ for the GID, and $a \approx 1 \times 10^{-6}$, $b \approx 1$, and $c \approx 1.1 \times 10^{-5}$ for the AID. Hence, the GID's computation time follows a power growth rate of $\mathcal{O}(m^{3.9})$, and the AID follows a linear growth rate of $\mathcal{O}(m)$. Clearly, as m increases, the AID is capable of delivering much lower latency in comparison with the GID. It is worth mentioning that ϵ progressively smaller than 0.5 is a better choice if $m > 12$.
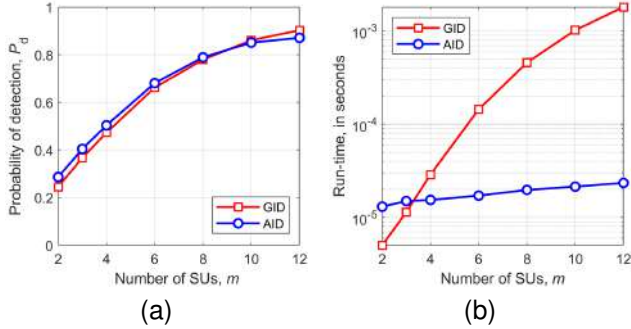
Fig. 3. (a) Probability of detection versus m, and (b) run-time versus m.

Fig. 5. (a) Probability of detection versus n, and (b) versus average SNR.

The influences of μ_K and η on P_d are shown in Fig. 3. It can be seen that the AID and GID perform close to each other for high values of μ_K, whereas the AID is considerably more advantageous at lower μ_K. Larger values of η reduces the performance of both detectors, as expected, since this situation produces larger discrepancies among the received signal powers across the SUs (it is worth noting that the SNR has been kept the same for any η). Nonetheless, the AID unveils a small advantage over the GID for all values of η.
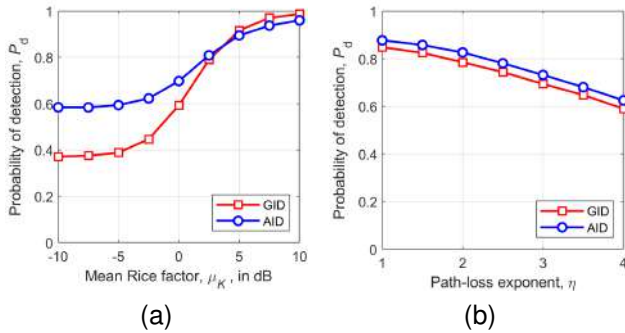

Fig. 6. (a) Probability of detection versus η, and (b) versus PU transmitter coordinates (x, y) for $(x = y)$.

V. CONCLUSIONS

This letter introduced the AID for centralized CSS and compared its performance with the GID, the first detector based on an income inequality index. The AID consistently outperforms the GID across various scenarios, with a time complexity that scales linearly with the number of SUs. Specifically, the AID operates with a computational time growth rate of $\mathcal{O}(m)$, in sharp contrast to the GID's power-law growth of $\mathcal{O}(m^{3.9})$. This difference in scaling has significant practical implications, as it enables the AID to deliver much lower latency as the number of users increases, making it a more efficient and scalable solution for real-world applications where fast and reliable spectrum sensing is critical.

Fig. 4. (a) Probability of detection versus μ_K, and (b) versus η.

Fig. 5 illustrates the influences of n and SNR on P_d. It can be seen that the performances of both detectors are improved as n increases, as expected, and that the GID is preferable for smaller number of samples, whereas the AID wins as n increases. Their respective advantages are not large, though. Regarding the SNR, the performances of both detectors improve as the SNR increases, as also expected, with a slight advantage of the AID at high SNR regimes.

Finally, Fig. 6 illustrates the influences of ρ and the PU transmitter coordinates on P_d. Fig. 6a demonstrates that both detectors are quite robust against the amount of noise power fluctuations, with the AID exhibiting a small advantage over the GID. In regard to the PU transmitter location, it can be seen in Fig. 6b that the performances of both detectors are reduced when $(x, y) < 2000$ m, keeping practically unchanged for larger distances. The performance reduction, which is an expected outcome, is owed to the fact that larger discrepancies among the received signal levels occur if the PU transmitter is close to the SUs.
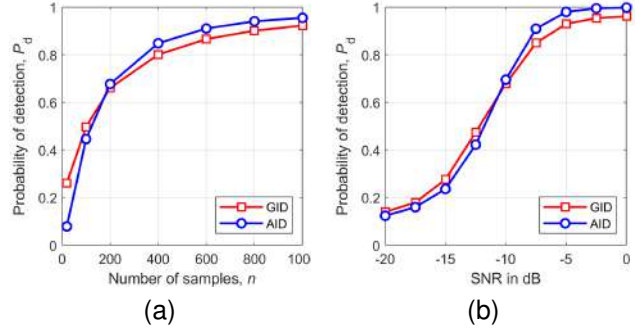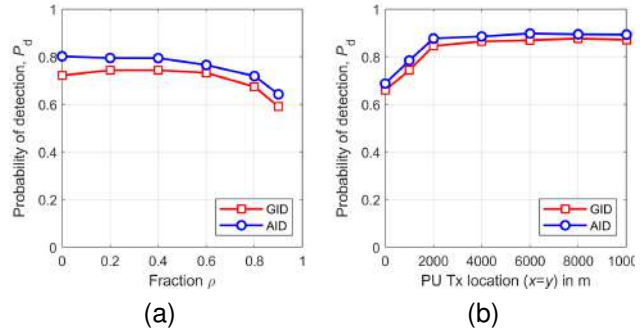
The hardware complexities of AID and GID, which can be fully assessed with accuracy only after they are implemented using field programmable gate array (FPGA) or application-specific integrated circuit (ASIC) designs [12]–[14], can be anticipated by comparing one of the AID test statistics (10), (11) or (12), with the GID test statistic (13): It can be inferred that the AID has the potential for attaining lower hardware complexity than the GID due to the smaller number of operations made to compute the test statistic.

It is also worth emphasizing that, for the sake of brevity, comparisons have been exclusively conducted between GID and AID. However, given the their performance similarity in numerous scenarios, one can readily infer the behavior of the AID against other detectors by examining in [6] how the GID compares with alternative techniques.

REFERENCES

[1] A. Nasser, H. Al Haj Hassan, J. Abou Chaaya, A. Mansour, and K.-C. Yao, "Spectrum sensing for cognitive radio: Recent advances and future challenge," *Sensors*, vol. 21, no. 7, 2021, doi: 10.3390/s21072408. [Online]. Available: https://www.mdpi.com/1424-8220/21/7/2408

[2] J. Mitola III and G. Q. Maguire Jr., "Cognitive radio: making software radios more personal," *IEEE Personal Commun. Mag.*, vol. 6, no. 4, pp. 13–18, Aug 1999, doi: 10.1109/98.788210.

[3] T. Yucek and H. Arslan, "A survey of spectrum sensing algorithms for cognitive radio applications," *IEEE Commun. Surveys Tuts.*, vol. 11, no. 1, pp. 116–130, 2009, doi: 10.1109/SURV.2009.090109.

[4] Y. Arjoune and N. Kaabouch, "A comprehensive survey on spectrum sensing in cognitive radio networks: Recent advances, new challenges, and future research directions," *Sensors*, vol. 19, no. 1, 2019, doi: 10.3390/s19010126.

[5] D. A. Guimarães, "Spectrum sensing: A tutorial," *Journal of Communication and Information Systems*, vol. 37, no. 1, pp. 10–29, Feb. 2022, doi: 10.14209/jcis.2022.2. [Online]. Available: https://jcis.sbrt.org.br/jcis/article/view/811

[6] ——, "Gini index inspired robust detector for spectrum sensing over Ricean channels," *Electronics Letters*, November 2018, doi: 10.1049/el.2018.7375.

[7] R. Neves Costa and S. Pérez-Duarte, "Not all inequality measures were created equal - The measurement of wealth inequality, its decompositions, and an application to European household wealth," European Central Bank, Statistics Paper Series 31, Dec 2019, doi: 10.2866/957288. [Online]. Available: https://www.ecb.europa.eu/pub/pdf/scpsps/ecb.sps31~269c917f9f.en.pdf

[8] D. A. Guimarães, "Hybrid fusion of Pietra-Ricci index detector information for cooperative spectrum sensing," *Ad Hoc Networks*, vol. 150, p. 103265, 2023, doi: 10.1016/j.adhoc.2023.103265. [Online]. Available: https://www.sciencedirect.com/science/article/pii/S1570870523001853

[9] S. Zhu, T. S. Ghazaany, S. M. R. Jones, R. A. Abd-Alhameed, J. M. Noras, T. Van Buren, J. Wilson, T. Suggett, and S. Marker, "Probability distribution of Rician K-factor in urban, suburban and rural areas using real-world captured data," *IEEE Trans. Antennas Propag.*, vol. 62, no. 7, pp. 3835–3839, Jul 2014, doi: 10.1109/TAP.2014.2318072.

[10] T. S. Rappaport, *Wireless Communications: Principles And Practice*, 2nd ed. Pearson Education, 2010. [Online]. Available: https://books.google.com.br/books?id=VmPT8B-5_tAC

[11] D. A. Guimarães, "MATLAB code to simulate the Atkinson index detector (AID) and the Gini index detector (GID) for spectrum sensing," September 2024. [Online]. Available: https://www.dropbox.com/scl/fi/ql4kmgo1xlb64t5ktm5dz/GIDvsAID.m?rlkey=0eip57w12q57ctgm8lcr2t9t8&dl=0

[12] R. B. Chaurasiya and R. Shrestha, "A new hardware-efficient spectrum-sensor VLSI architecture for data-fusion based cooperative cognitive-radio network," *IEEE Trans. Very Large Scale Integr.*, vol. 29, no. 4, pp. 760–773, April 2021, doi: 10.1109/TVLSI.2021.3059260.

[13] D. A. Guimarães, E. J. T. Pereira, and R. Shrestha, "Resource-efficient low-latency modified Pietra-Ricci index detector for spectrum sensing in cognitive radio networks," *IEEE Trans. Veh. Technol.*, pp. 1–15, 2023, doi: 10.1109/TVT.2023.3269345.

[14] E. J. T. Pereira, D. A. Guimarães, and R. Shrestha, "VLSI architectures and hardware implementation of ultra low-latency and area-efficient Pietra-Ricci index detector for spectrum sensing," *IEEE Trans. Circuits Syst. I, Reg. Papers.*, vol. 71, no. 5, pp. 2348–2361, 2024, doi: 10.1109/TCSI.2024.3376952.

APPENDIX

The square root of a complex quantity $r_{ij} = a_{ij} + jb_{ij}$ is

$$\sqrt{r_{ij}} = \sqrt{|r_{ij}|}\cos(\theta_{ij}/2) + j\sqrt{|r_{ij}|}\sin(\theta_{ij}/2),$$

where $\theta_{ij} = \arctan(b_{ij}/a_{ij})$. When $\epsilon = 0.5$ in (10), from the conjugate symmetry of $\mathbf{R}$ and the above result, we obtain

$$\sum_{i=1}^{m}\sum_{j=1}^{m}\sqrt{r_{ij}} = \sum_{i=1}^{m}\sum_{j=1}^{m}\Re(\sqrt{r_{ij}}) = \sum_{i=1}^{m}\sum_{j=1}^{m}\sqrt{|r_{ij}|}\cos(\theta_{ij}/2).$$

Applying the trigonometric identity $\cos(\theta_{ij}/2) = \{[1 + \cos(\theta_{ij})]/2\}^{0.5}$ and the fact that $\cos(\theta_{ij}) = a_{ij}/|r_{ij}|$, after some simple manipulations it is found that

$$\sum_{i=1}^{m}\sum_{j=1}^{m}\sqrt{r_{ij}} = \sum_{i=1}^{m}\sum_{j=1}^{m}\sqrt{\frac{|r_{ij}| + \Re(r_{ij})}{2}}.$$

Dayan Adionel Guimarães received his Master and Ph.D. degrees in Electrical Engineering from the State University of Campinas (Unicamp), Brazil, in 1998 and 2003, respectively. He is a Researcher and Senior Lecturer at the National Institute of Telecommunications (Inatel) in Brazil. His research is currently directed towards wireless communications in general, specifically radio signal propagation, digital transmission, spectrum sensing, dynamic spectrum access, and random signal processing.